Nanoscale Advances

ROYAL SOCIETY OF CHEMISTRY

PAPER

View Article Online
View Journal | View Issue

Check for updates

Cite this: *Nanoscale Adv.*, 2025, **7**, 4636

Experimental research on fungal inhibition using dissolving microneedles of terbinafine hydrochloride nanoemulsion for beta-1,3-glucanase

Huilin Wang,[a] Yan Wang,†[a] Jianing Liu,[a] Yonghua Qi,[c] Weitong Sun,[a] Hongbin Qiu,*[a] Yu Zhang *[ab] and Yang Ping *[ab]

Objective: Onychomycosis is characterized by high transmission and low recovery rates, leading to a lack of optimal treatments. This study used dissolving microneedles as drug carriers to design dual-loaded DMN patches with β-1,3-glucanase and terbinafine hydrochloride nanoemulsion. *Methods*: Dissolving microneedles of terbinafine hydrochloride nanoemulsion for beta-1,3-glucanase (Gls–TBH-NE–DMN) were prepared using the centrifugal molding method. Parafilm®, weight method, mouse skin puncture experiments, and mouse skin tissue sections were used to evaluate the mechanical properties of Gls–TBH-NE–DMN. Gls–TBH-NE–DMN was tested for its *in vitro* anti-*Candida* albicans susceptibility, ability to inhibit fungal cell wall synthesis, and fungal biofilm penetration and inhibition capabilities. The *in vivo* inhibitory effect of Gls–TBH-NE–DMN on fungi was studied using a rabbit nail infection model. *Results*: Gls–TBH-NE–DMN exhibited a penetration rate of 98% on skin simulants and a compressive bending resistance of 12.75%. It was nonirritating to the dorsal skin of mice, with no edema or erythema on the surface of the skin, suggesting a good safety profile. The accumulative release of Gls–TBH-NE–DMN at 72 h was 78.74% ± 0.64%, and that of terbinafine hydrochloride dissolving microneedles was 49.52% ± 0.80%. In the *in vitro* transdermal permeation experiment, the cumulative transdermal permeation of Gls–TBH-NE–DMN at 72 h was 73.21% ± 0.84% and that of terbinafine hydrochloride (TBH) was 20.57% ± 0.98%. *In vitro* inhibition of *C. albicans* showed that the lowest inhibitory concentration in the Gls–TBH-NE–DMN group was 512 μg mL^{-1}. Furthermore, experiments showed that Gls–TBH-NE–DMN could effectively inhibit fungal cell wall synthesis and disrupt the *C. albicans* biofilm, inhibiting fungal growth. *Conclusions*: Gls–TBH-NE–DMN prepared in this study provides new ideas for treating skin fungal diseases and for developing antimicrobial drug formulations.

Received 18th February 2025
Accepted 5th June 2025

DOI: 10.1039/d5na00163c

rsc.li/nanoscale-advances

Open Access Article. Published on 06 June 2025. Downloaded on 4/3/2026 4:50:10 AM. This article is licensed under a Creative Commons Attribution-NonCommercial 3.0 Unported Licence.

Introduction

Onychomycosis is a fungal disease caused by dermatophytes, nondermatophyte molds, and yeasts. Onychomycosis accounts for 30% of all fungal skin and nail infections, with a prevalence of 50% among patients with tinea pedis.[1–6]

The preferred treatment for fungal infections in China is oral terbinafine hydrochloride (TBH). TBH is available in topical and oral delivery modes in clinical applications. TBH has been a mainstream drug for treating superficial fungal infections of the skin, especially dermatophyte infections, as a first-line therapeutic agent.[7–9] However, the current clinical applications of TBH are mainly divided into oral drug therapy, transdermal drug therapy, and physiotherapy. Among these applications, oral treatment leads to serious adverse effects, such as gastrointestinal irritation, increased risk of hepatotoxicity, and congestive heart failure,[10–12] limiting the use of TBH. In contrast, topical application of TBH creams or gels is susceptible to the barrier effect of the stratum corneum of the skin, resulting in low skin penetration of the drug. Physical laser therapy can only temporarily improve the appearance of the nail without completely eradicating onychomycosis.[13] To mitigate these limitations in treating onychomycosis, we explored the pathogenesis of the disease.

Owing to the limited effectiveness of cell-mediated immunity in nails, trauma to the nail or cracks in the skin can allow the fungi to invade the space between the nail cap and the bed. The protein hydrolyzing-, keratin hydrolyzing-, and lipolytic

[a]*College of Pharmacy, Jiamusi University, Jiamusi, 154007, Heilongjiang, China. E-mail: 1957752730@qq.com; 2813149909@qq.com; 1179869656@qq.com; weitongsun@163.com; qhbin63@163.com*

[b]*Heilongjiang Pharmaceutical Research Institute, Jiamusi, 154007, Heilongjiang, China. E-mail: zhangyu@jmsu.edu.cn; 18245482328@163.com*

[c]*Heilongjiang University of Chinese Medicine Jiamusi College, Jiamusi, 154007, Heilongjiang, China. E-mail: 723555033@qq.com*

† These authors contributed equally to this work and are co-first authors.

© 2025 The Author(s). Published by the Royal Society of Chemistry

Open Access Article. Published on 06 June 2025. Downloaded on 4/3/2026 4:50:10 AM. This article is licensed under a Creative Commons Attribution-NonCommercial 3.0 Unported Licence.

activating-enzymes produced by fungi degrade keratin in the nail plate, which in turn promotes the invasion of the fungi into the nail plate and causes the cuticular layer of the skin of the fingernail (toenail) to become infected with fungi.[14–16] The cell wall is the outermost protective membrane of fungal cells and can reduce their sensitivity to antifungal drugs, resulting in less effective antifungal drug therapy. The fungal cell wall comprises mannoprotein, β-glucan, and chitin. Among these, β-glucan is the skeleton structure of the fungal cell wall and plays a major supporting role in the fungal cell wall. β-1,3-Glucanase (Gls) can inhibit the synthesis of β-1,3-glucan, promoting the exposure of pathogen factors and activating the immune defense mechanisms, thus hindering the synthesis of the fungal cell wall.[17–19] The difficulty in eradicating onychomycosis and the high incidence of secondary morbidity were due to the formation of fungal biofilms outside the fungal cells. Fungal biofilms consist of a multicellular community protected by an extracellular matrix, which increases host cell resistance to antifungal drugs.[20–22] Consequently, Gls can be used as antifungal target substances.

Tan *et al.*'s team[23–28] extensively demonstrated that Gls can interfere with fungal biofilm formation and exhibited the highest efficacy on the removal of a mature biofilm, thereby increasing the susceptibility of fungal cells to antifungal drugs. TBH is an acrylamide antifungal drug that specifically interferes with the early biosynthesis of fungal ergosterol. TBH blocks squalene epoxidation during the formation of fungal biofilms. This drug has a highly selective inhibitory effect on fungal squalene cyclooxygenase, preventing the generation of fungal biofilms and achieving fungicidal and antibacterial effects.[29–34] The greatest innovation of this study was the combination of two drugs with microneedles, which punctured the skin directly, bypassing the stratum corneum barrier and delivering the antifungal drug through the proximal nail folds of the nails to the subcutaneous nail matrix area. This combination provides antifungal treatment from the source of the fungal infection, allowing a greater volume of the drug to reach the affected area directly.

The WHO released its first list of fungal priority pathogens in 2022, classifying *Candida albicans* as critical.[35] *C. albicans* is responsible for 70% of all cases of onychomycosis[36–38] because the biofilms of *C. albicans* adhere firmly to the surface of fungal cells during their formation. This adhesion reduces the sensitivity of fungal cells to antifungal drugs, making them more resistant and leading to the difficult eradication of onychomycosis.[39–41] Therefore, in this study, *C. albicans* was used as a model strain to construct a rabbit onychomycosis model for *in vitro* antifungal experimental studies.

Soluble microneedles, also known as dissolvable microneedles (DMN), are an innovative method of directly delivering drugs or active ingredients into the deeper layers of the skin using transdermal technology. When the DMN is inserted into the skin, the tip of the needle spontaneously degrades, releasing the loaded into the drug, which is then directly absorbed for precise drug delivery.[42–47] The release rate of DMN was mainly related to the drug and its dosage form. Additionally, DMNs can be loaded with modified drugs and drug carriers, such as hydrophilic and lipophilic functional groups, enzyme chains, drug-loaded nanoparticles, nanoemulsions (NE), and micelles. Nanoemulsions (NE) are used as nanosized drug carriers to improve the solubility of insoluble drugs and increase drug dispersion.[48–52] Whereas TBH has poor water solubility, NE has the advantages of improving drug solubility and increasing drug biofilm permeability and bioavailability. The molecular weight of 20–40 w hyaluronic acid is a water-soluble matrix toughness material that improves the flexibility of DMN. Polyvinyl alcohol and polyvinyl pyrrolidone K30 are synthetic biodegradable polymer matrix materials, PVA is a ductile material and polyvinyl pyrrolidone K30 is a brittle material, which improves the mechanical strength of DMN. Multiple teams, including Hou, study microneedle delivery of antibacterial drugs to treat diabetic wounds, fungicide-targeted microneedles for wound healing and microtargeting of fungal keratitis.[53–56]

In summary, a combination of the two drugs TBH and Gls was selected for this experiment, and TBH was prepared as oil-in-water NE using oil emulsification. The dissolving microneedles of terbinafine hydrochloride nanoemulsion for beta-1,3-glucanase (Gls–TBH-NE–DMN) were prepared by loading terbinafine hydrochloride nanoemulsion (TBH-NE) and Gls into DMN carriers using the centrifugal insertion method to avoid side effects from oral TBH tablets and to broaden the range of people for whom it was indicated. Furthermore, Gls–TBH-NE–DMN inhibits the formation of fungal biofilms through Gls, improves the sensitivity of fungal cells to the drug, increases the concentration of local drug therapy, and further improves the treatment outcome of onychomycosis.

Materials and methods

Materials and equipment

Polyvinyl alcohol (model: 224), hyaluronic acid (molecular weight: 20–40 w), polyvinyl pyrrolidone K30 (molecular weight: 4 w), terbinafine hydrochloride (purity: 98%), PEG-40 hydrogenated castor oil (HLB: 13–14, pH: 5.0–7.0), tween 80, 1,2-propylene glycol, caprylic triglyceride, RPMI-1640, kerosene and 4% paraformaldehyde were purchased from Shanghai MACKLIN Biochemical Technology Co., China. Parafilm® (Bemis Company, Inc.). Phosphate-buffered saline (PBS) powder (Sharp Biotechnology, Hangzhou, China). Sodium dodecyl sulfate (Tianjin Kaitong Chemical Reagent, China. Methanol) and acetonitrile (Thermo Fisher Scientific Co., China). Purified water (homemade in the laboratory). β-1,3-Glucanase (≥2000 units mg^{-1}), fluorescein isothiocyanate-concanavalin A (FITC-ConA) and propidium iodide (PI) (HPLC ≥94%) were purchased from Sigma-Aldrich, Shanghai, China. Terbinafine hydrochloride cream (Hunan Dino Pharmaceutical Co. Ltd., China). *C. albicans* (Strain No. BNCC 299343), YM medium powder and agar powder were purchased from BeNa Culture Collection, China, 2% lidocaine hydrochloride (Huamu Animal Health Products Co. Ltd., Jilin, China). PLANK decalcification solution (Homemade in the laboratory). Methylprednisolone sodium succinate (Pfizer Pharmaceuticals Ltd.).

Open Access Article. Published on 06 June 2025. Downloaded on 4/3/2026 4:50:10 AM. This article is licensed under a Creative Commons Attribution-NonCommercial 3.0 Unported Licence.

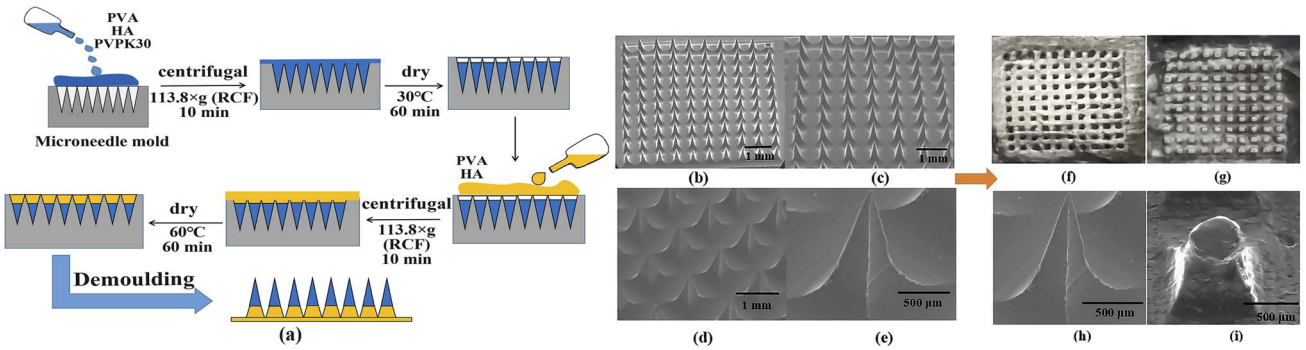

Fig. 1 Preparation, morphological characterization and mechanical property evaluation of terbinafine hydrochloride nanoemulsion for beta-1,3-glucanase (Gls–TBH-NE–DMN): (a) preparation process of Gls–TBH-NE–DMN, (b)–(e) morphology of Gls–TBH-NE–DMN, (f and g) mechanical strength examination of Gls–TBH-NE–DMN, and (h and i) pressure performance examination of Gls–TBH-NE–DMN.

Instrumentation used in the study included a polydimethylsiloxane mold (10 × 10 arrays, needle height 800 μm, Micropoint Technologies PTE LTD, Singapore), an electronic analysis balance (Hengping Science Instrument Co. Ltd., Shanghai, China), a benchtop low-speed centrifuge (Xiangyi Laboratory Instrument Development Co. Ltd., Hunan, China), an electric air drying box (Experimental Instrument Factory Co. Ltd., Shanghai, China), a heat collecting constant temperature heating magnetic stirrer (Yuhua Instrument Co. Ltd., Gongyi, China), an ultrasonic cell crusher (Xinzhi Biotechnology Co. Ltd., Ningbo, China), a water bath constant temperature oscillator (Zhongbei Instrument Co. Ltd., Changzhou, China), a high-temperature difference thermal analyzer (Netzsch Germany), a Fourier transform infrared spectrometer (Guangdong Technology Co. Ltd., Tianjin China), a high-performance liquid chromatograph (Agilent Technology Co. Ltd., USA), an intelligent transdermal tester (Pharmacopeia Standard Instrument Factory, Tianjin, China), a fluorescence inverted microscope (Leica Instrument Co. Ltd., German), a field emission scanning electron microscope (Electronics Co. Ltd., Japan), an optical microscope (Caikang Optical Instrument Co. Ltd., Shanghai, China), and a texture analyzer (Hengpin Electromechanical Technology Co. Ltd., Jinan, China).

Experimental animals

Twenty Kunming male mice, SPF grade, weekly age: 3–5 weeks were purchased from the Department of Laboratory Animal Science, Harbin Medical University, Harbin City, Heilongjiang Province, China. License No.: SCXK (Black) 2019-001. Thirty white male New Zealand rabbits (weekly age: 3–4 weeks) were purchased from the Department of Laboratory Animal Science, Harbin Medical University, Harbin City, Heilongjiang Province, China.

Preparation of Gls–TBH-NE–DMN

Weigh 1.80 g of PEG-40 hydrogenated castor oil, 0.60 g of Tween 80, 0.80 g of 1,2-propylene glycol, 1.024 g of caprylic triglyceride, and 0.13 g of TBH were placed in a beaker and stirred at a constant temperature of 50 °C until completely dissolved, and then purified water was added into the above-mixed system at a constant speed, and when the system became a light blue homogeneous solution, it was put into an ice-water bath, and the power was 60%, and the TBH-NE was dispersed by sonication for 10 min. The power was 60%, ultrasonic dispersion was performed for 10 min, and TBH-NE was obtained.

Polyvinyl alcohol was weighed and dissolved in Gls solution, hyaluronic acid was dissolved in purified water, polyvinyl pyrrolidone K30 was dissolved in TBH-NE, and polyvinyl alcohol, hyaluronic acid, and polyvinyl pyrrolidone K30 solution were dissolved in the refrigerator for 30–40 min. The three-drug solution was mixed uniformly in a ratio of 1 : 1 : 4. The solution was then poured into a polydimethylsiloxane mold and centrifuged at 113.8 × *g* (RCF) for 10 min. After centrifugation and drying in an oven at 30 °C for 60 min, the backing layer solution was dropped into the polydimethylsiloxane mold, centrifuged at 113.8 × *g* (RCF) for 10 min, and placed in the drying oven at 60 °C for another 60 min. The Gls–TBH-NE–DMN arrays were obtained by removing and demolding the arrays (Fig. 1a).

Morphological characterization of Gls–TBH-NE–DMN

Appearance of Gls–TBH-NE–DMN. The appearance of Gls–TBH-NE–DMN prepared using the centrifugal-in-mold method was examined. The microscopic morphology of the Gls–TBH-NE–DMN needles, tip curvature, tip integrity, and the needle puncture rate of the Gls–TBH-NE–DMN arrays were examined using a texture analyzer, and the tip compatibility with the backing layer was assessed.

Observation under a field emission scanning electron microscopy. The tip of Gls–TBH-NE–DMN was placed upward on the carrier stage, and the appearance morphology of Gls–TBH-NE–DMN was observed using field emission scanning electron microscopy (FESEM) with a 15.0 kV LED.

Evaluation of the mechanical properties of Gls–TBH-NE–DMN

Insertion performance study. Using a Parafilm® film as a skin analog,[57] Parafilm® puncture experiments were

© 2025 The Author(s). Published by the Royal Society of Chemistry

Open Access Article. Published on 06 June 2025. Downloaded on 4/3/2026 4:50:10 AM. This article is licensed under a Creative Commons Attribution-NonCommercial 3.0 Unported Licence.

performed to evaluate the mechanical strength of Gls–TBH-NE–DMN. Four layers of Parafilm® film with a thickness of 0.5–1 mm were laid flat on the foam board. After puncturing the Parafilm® film vertically with the tip of the Gls–TBH-NE–DMN needle, a uniform force of 11 N was applied with the texture analyzer.[58] The needle was then removed after being pressed for 30–60 s. This process was repeated five times in parallel operations. The number of layers punctured by the Gls–TBH-NE–DMN and the number of holes in each layer was recorded.

Examination of pressure performance. To evaluate the toughness of the Gls–TBH-NE–DMN using a pressure performance examination, the Gls–TBH-NE–DMN needle was placed tip down on the smooth flat surface, an applied pressure of 11 N with the texture analyzer and a flat surface was placed on the back of the Gls–TBH-NE–DMN to make the force on the Gls–TBH-NE–DMN uniform. The Gls–TBH-NE–DMN needle was removed after 1–2 min and operated five times in parallel to observe changes in the Gls–TBH-NE–DMN needle tip and height.

Dissolution experiments of Gls–TBH-NE–DMN in mouse skin. Gls–TBH-NE–DMN was applied to the dorsal skin of mice, and the force of 11 N was applied evenly using a texture analyzer, and the sample was pulled out after 0, 30, 120, and 300 s. The operation was conducted in parallel three times, and Gls–TBH-NE–DMN tip height changes were observed using FESEM to assess the dissolution of Gls–TBH-NE–DMN tips within mice skin.

Skin puncture experiments of Gls–TBH-NE–DMN. The skin on the back of 5 × 5 cm^2 mice was selected for hair removal, exposing smooth skin on the back of the mice. The Gls–TBH-NE–DMN was placed perpendicular to the skin on the back of the mice, and a texture analyzer was used to pierce the skin with a force of 11 N. Gls–TBH-NE–DMN was obtained after 2–5 min, operated in parallel three times, and the number of pinholes in the skin on the back of the mice was observed.

Skin histology experiment of Gls–TBH-NE–DMN mice. The Gls–TBH-NE–DMN was applied to the dorsal skin of mice, and a force of 11 N was applied by a texture analyzer to puncture the Gls–TBH-NE–DMN into the dorsal skin of mice. The Gls–TBH-NE–DMN patch was removed after 5 min, and the skin at the puncture site was removed and immersed in paraformaldehyde for 24 h. After 24 h, hematoxylin and eosin staining were performed, and specimens were observed under a microscope.

Skin safety evaluation of Gls–TBH-NE–DMN

Skin-healing experiment of Gls–TBH-NE–DMN. The Gls–TBH-NE–DMN was perpendicularly inserted into the dorsal spinal cord of mice using a texture analyzer with a force of 11 N for 30–60 s. The needle eye of the dorsal skin of mice was observed at 0, 5, 10, 15, and 30 min, and the dorsal skin of mice was operated three times in parallel to evaluate the healing time of the dorsal skin of the mice and to verify the safety of Gls–TBH-NE–DMN.

Skin irritation evaluation of Gls–TBH-NE–DMN. Twenty mice were randomly divided into four groups of five each. The skin of the 5 × 5 cm^2 dorsal spine of mice was selected 24 h before drug administration, and dehairing was performed. Saline was applied to the blank group, an appropriate amount of TBH-NE was applied to the TBH-NE group, one patch of Gls–TBH-NE–DMN was given to the Gls–TBH-NE–DMN group, and an appropriate amount of TBH cream was applied to the positive control group. The status of the dorsal skin of mice was observed after 0, 24, 48, 72, 96, and 120 h, and local reactions in the dorsal skin were recorded.

Differential scanning calorimetry and Fourier transform infrared spectroscopy (FTIR) study of Gls–TBH-NE–DMN. Differential scanning calorimetry (DSC) was used to determine the heat absorption peaks of TBH, blank DMN powder, Gls–TBH-NE–DMN powder, and physical mixtures of TBH and blank DMN powder. The samples were weighed, placed in a crucible and scanned in the range of 20–300 °C at a heating rate of 10 °C min^{-1}, with a N_2 flow rate of 50 mL min^{-1}.

FTIR spectroscopy was used to determine the TBHs and physical mixtures of TBH, blank DMN, Gls–TBH-NE–DMN, and blank DMN. The samples to be tested were prepared using the KBr compression method and scanned using infrared spectroscopy in the range of 400–4000 cm^{-1}.

Establishment of analytical methodology for TBH *in vitro* release

Liquid chromatography conditions. The chromatographic column was a reversed-phase Eclipse XDB-C-18 column (250 mm × 4.6 mm; 5 μm) with a column temperature of 25 °C. High-performance liquid chromatography conditions were mobile phase A: methanol, B: acetonitrile, and C: water. The gradient elution conditions were as follows: 0–2 min, 40% A and 50% B; 2–6 min, 65% A and 15% B; and 6–10 min, 40% A and 50% B. The injection volume was 10 μL, the flow rate was 0.8 mL min^{-1}, and the detection wavelength was 224 nm.

Linear relation. Accurately weigh 25.00 mg of TBH standard, put it in a 100.00 mL volumetric flask, add phosphate buffer solution (PBS) containing 1% sodium dodecyl sulfate (SDS) with pH of pH 7.4 to make constant volume calibration, and ultrasonically dissolve it for 10 min to prepare 250.00 μg mL^{-1} TBH mother liquor.

Accurately suck 0.40, 0.80, 1.5, 2.40, 3.20 and 4.80 mL of TBH mother liquor, and put them into 10.00 mL volumetric flasks, respectively. PBS solution with pH 7.4 containing 1% SDS was calibrated at a constant volume and 10.00, 20.00, 40.00, 60.00, 80.00 and 120.00 were obtained. Filter with 0.22 μm microporous membrane, as detected by HPLC, recorded the peak area, and performed linear regression with concentration (X) as the abscissa and peak area (Y) as the ordinate.

Measurement of the encapsulation rate and drug loading. A piece of Gls–TBH-NE–DMN prepared from different batches was dissolved in a 70% methanol aqueous solution. The 70% methanol aqueous solution was fixed and filtered through a 0.22 μm microporous membrane. The TBH content of the microneedles was determined using the method described above.

Open Access Article. Published on 06 June 2025. Downloaded on 4/3/2026 4:50:10 AM. This article is licensed under a Creative Commons Attribution-NonCommercial 3.0 Unported Licence.

$$W_{\text{drug capacity}}\ (\%) = \frac{W_{\text{total encapsulated and unencapsulated drug}} - W_{\text{unencapsulated drug quantity}}}{W_{\text{Gls-TBH-NE-DMN gross weight}}} \times 100\% \quad (1)$$

A piece of Gls–TBH-NE–DMN prepared from different batches was dissolved in 70% methanol aqueous solution and centrifuged at 783 × *g* (RCF) for 10 min. After centrifugation, 1.5 mL of the supernatant was collected in a 10 mL volumetric flask; the 70% methanol aqueous solution was fixed and filtered through a 0.22 μm microporous filter membrane. Subsequently, the TBH encapsulation rate in the Gls–TBH-NE–DMN was determined as described above. The TBH encapsulation rate in the DMN was determined as described above.

$$W_{\text{encapsulation ratio}}\ (\%) = \frac{C_{\text{total drug content}} - C_{\text{free drug content}}}{C_{\text{total drug content}}} \times 100\% \quad (2)$$

***In vitro* release degree experiment of Gls–TBH-NE–DMN.** *In vitro* release degree experiments of terbinafine hydrochloride dissolving microneedles (TBH–DMN) and Gls–TBH-NE–DMN were performed using the dialysis method. Precisely 15 mL of the TBH–DMN and Gls–TBH-NE–DMN solutions were pipetted and transferred into a dialysis bag with a molecular weight of 14 000 Da. The dialysis bag was placed in 400.00 mL of phosphate-buffered saline (PBS) solution release medium containing 1% sodium dodecyl sulfate at pH 7.4 and subjected to thermostatic shaking at a rate of 0.068 × *g* (RCF) and temperature of 37 °C ± 0.5 °C. Samples of 3.0 mL were collected at 0.08, 0.25, 0.5, 1, 2, 4, 6, 8, 12, 24, 48, and 72 h, replenishing the same release medium volume.[59,60]

Cumulative drug release (%) was determined by HPLC and analyzed as a function of time (t, h). The accumulative release (Q_n, μg mL^{-1}) was calculated using formula (3), and the accumulative release (%) was calculated using formula (4):

$$Q_n = C_n \times V_0 + \sum_{i=1}^{n=1} C_i \times V_i \quad (3)$$

$$Q_n^* = Q_n / Q_{\text{cast}} \times 100\% \quad (4)$$

The $t - Q_n^*$ curve was plotted with t as the horizontal coordinate and *in vitro* cumulative release degree (Q_n^*) as the vertical coordinate, and the curve was fitted to calculate the release equation.

***In vitro* transdermal permeation experiment of Gls–TBH-NE–DMN.** *In vitro* transdermal permeation experiments of TBH, dissolving microneedles of terbinafine hydrochloride nanoemulsion (TBH-NE–DMN), Gls–TBH-NE–DMN, and commercially available TBH creams were conducted using the Franz diffusion cell method. The skin was immobilized in the middle of the upper and lower pools, with the keratin surface facing the release pool and the dermal surface facing the receiving pool. Subsequently, fifteen millilitre of PBS solution at pH 7.4 containing 1% sodium dodecyl sulfate was added to the receiving pool, and 3.0 mL of TBH, TBH–NE–DMN, Gls–TBH-NE–DMN, and commercially available TBH cream solution were added to the release pool. The diffusion cell was placed in a constant-temperature water bath at 37 °C ± 0.5 °C with a stirring rate of 0.38 × *g* (RCF), and 1.5 mL of samples were collected at regular intervals of 0.5, 1, 2, 3, 4, 6, 8, 10, 12, 24, 48, and 72 h. The sample was replenished with the same volume of fresh receiving solution, filtered through a 0.22 μm microporous membrane, and analyzed according to the high-performance liquid chromatography conditions described in Section 2.11.

The cumulative transdermal permeation volume Q_n (μg cm^{-2}) and cumulative transdermal transmittance Q_n^* (%) were calculated for each group, and the relationship between the cumulative transdermal transmittance and time (t, h) was examined. The cumulative transdermal permeation volume Q_n (μg cm^{-2}) was calculated using formula (5), and the cumulative transdermal transmittance Q_n^* (%) was calculated using formula (6):

$$Q_n = \left(VC_n + \sum_{i=1}^{n=1} C_i V_i \right) \Big/ A \quad (5)$$

$$Q_n^* = Q_n / Q_{\text{cast}} \times 100\% \quad (6)$$

The $t - Q_n^*$ curve was plotted with t as the horizontal coordinate and *in vitro* cumulative release degree (Q_n^*) as the vertical coordinate, and the curve was fitted to calculate the release equation.

***In vitro* fungal inhibition experiment of Gls–TBH-NE–DMN.** Experimental grouping: the antifungal experiments were divided into a control group: Con, model group: Mod, TBH–DMN administration group: TBH–DMN, Gls–TBH-NE–DMN administration group: Gls–TBH-NE–DMN, and positive control group: PC. The Microneedle group is administered by a texture analyzer.

Minimum inhibitory concentration experiments. The RPMI-1640 medium was used to dilute the solution concentration of the TBH–DMN, Gls–TBH-NE–DMN, and PC groups in gradient to 1024 μg mL^{-1} (1,024, 512, 256, 128, 64, 32, 16, 8, 4, and 2 μg mL^{-1}). Subsequently, one hundred microlitres of the corresponding drug solution (TBH–DMN, Gls–TBH-NE–DMN, and PC solution) were added to wells 1–10. The eleventh well was set as the growth control well containing 200 μL of bacterial solution, and the 12th well was set as the sterile control well containing 200 μL of RPMI-1640 medium. Subsequently, one hundred microlitres of a *C. albicans* solution were added to wells 1–10, and the solution was gently blown to mix with the fungal solution. The ninety-six-well plates were incubated in a constant-temperature incubator at 30 °C for 24–48 h. Three parallel wells were set up for each drug concentration. At the end of the incubation, the spiked wells were compared with the growth control wells, and the drug concentration corresponding

© 2025 The Author(s). Published by the Royal Society of Chemistry

Open Access Article. Published on 06 June 2025. Downloaded on 4/3/2026 4:50:10 AM. This article is licensed under a Creative Commons Attribution-NonCommercial 3.0 Unported Licence.

to the complete inhibition of mycelial growth was determined as the minimum inhibitory concentration (MIC).[61–63]

The incubated 96-well test plate was removed, and the solution was aspirated into the wells at concentrations higher than the MIC. The wells were coated on YM agar medium and incubated at a constant temperature incubator at 30 °C for 24–48 h. The number of colonies in the medium was counted at the end of incubation. The value of the corresponding drug concentration was MIC when no colonies grew or fewer than three colonies were present. Each drug concentration was tested in triplicate.

Drug-sensitive paper slide experiments. First, six-millimetre round filter paper sheets were prepared, autoclaved, and dried for use as spare parts. Subsequently, ten microlitres of Con, TBH–DMN, Gls–TBH-NE–DMN, and PC solutions were pipetted through micropipettes. Drops were placed on dry and sterile circular filter paper sheets, allowed to dry in a sterile ultra-clean bench after complete absorption, dispensed into sealed sterile vials, placed in the refrigerator, and kept for spare use.

Subsequently, twenty microlitres of a 1×10^6 CFU mL^{-1} *C. albicans* solution was dropped into the center of the YM agar medium and spread evenly. The coated medium was evenly divided into four areas: *a*, *b*, *c*, and *d*. Corresponding drug-sensitive paper tablets were placed in the center of each area and incubated at 30 °C for 24–48 h in an incubator at constant temperature. When the incubation was completed, the size of the circle of inhibition on the paper sheet was measured to determine the inhibitory effect of the drugs on the fungal strains, and each drug paper tablet was repeated three times. The mean diameter value of the inhibition circle was measured.[63]

Inhibition experiments of fungal cell wall synthesis. To each of the four sterile test tubes, five hundred microlitres of 1×10^6 CFU mL^{-1} *C. albicans* were added. Subsequently, one thousand microlitres of Con, TBH–DMN, Gls–TBH-NE–DMN, and PC solution were added. After mixing the fungal and drug solutions evenly, four test tubes were incubated in a constant-temperature incubator at 30 °C for 24–48 h of static culture. Subsequently, two hundred and fifty microlitres of paraffin were added to four test tubes and incubated at 30 °C for 60 min. At the end of the incubation, the visual assessment was made based on the height and fineness of the foam produced in the test tube and the degree of emulsification. The degree of fungal cell wall inhibition was determined, and each drug solution was repeated three times.

Fluorescein isothiocyanate-concanavalin a fluorescence staining. First, one hundred microlitres of 1×10^6 CFU mL^{-1} *C. albicans* solution was added to each well of a 96-well plate, and 100 μL of TBH–DMN, Gls–TBH-NE–DMN, and PC solution were added. Each drug concentration was replicated three times and incubated at 30 °C for 24–48 h. At the end of incubation, the culture medium and unadhered cells in the well plates were discarded, and the cells were washed three times with PBS. Subsequently, one hundred microlitres of fluorescein isothiocyanate-concanavalin A (FITC-ConA) fluorescent dye was added to each well, and the cells were incubated for 30 min at 37 °C in a constant temperature incubator protected from light. After incubation, the unbound dye was removed by washing with a sterile PBS solution under a fluorescence-inverted microscope, and the formation of fungal biofilms was observed.[64–66]

Propidium iodide (PI) fluorescent staining. First, one hundred microlitres of a 1×10^6 CFU mL^{-1} *C. albicans* solution was added to each well of a 96-well plate, and 100 μL of TBH–DMN, Gls–TBH-NE–DMN, and PC solution were added. Each drug concentration was replicated three times and incubated at 30 °C for 24–48 h. At the end of incubation, the culture medium and unadhered cells were discarded from the well plates and washed three times with a sterile PBS solution. Subsequently, twenty microlitres of PI fluorescent dye were added to each well, and the mixture was incubated for 30 min at 37 °C in a thermostatic incubator protected from light. After incubation, the unbound dye was washed with sterile PBS solution under a fluorescent-inverted microscope, and the formation of fungal biofilms was observed.[64–66]

In vivo fungal inhibition experiment of Gls–TBH-NE–DMN

Animal modeling and drug delivery therapy. Animal grouping: thirty white New Zealand rabbits were randomly divided into five groups: control group: Con, model group: Mod, TBH–DMN administration group: TBH–DMN, Gls–TBH-NE–DMN administration group: Gls–TBH-NE–DMN, and positive control group: PC. The Microneedle group is administered by a texture analyzer.

The rabbit onychomycosis model was based on the literature.[67,68] Each New Zealand white rabbit was administered an intramuscular injection of methylprednisolone sodium succinate in the forelimb once a week for 4 weeks. In the third week, 1×10^6 CFU mL^{-1} *C. albicans* suspension was injected into the proximal nail folds of the left and right forepaws of rabbits. The rabbit's paws were wrapped in gauze and moistened with sterile water, and the outside was secured with a rubber sleeve for 2 weeks. The gauze was removed in the fourth week of treatment. The Con group applied the appropriate amount of saline, the Mod group had no administration, the TBH–DMN group was given TBH–DMN patch treatment by applying the TBH–DMN patch to the proximal nail folds of rabbit nails, the Gls–TBH-NE–DMN group was treated by applying Gls–TBH-NE–DMN patch to the proximal nail folds of rabbit nails, and the PC group was coated with a commercially available TBH cream. The treatment was administered continuously for 2 weeks.

Local anesthesia was administered *via* a 2% lidocaine hydrochloride injection in the sixth week. After anesthesia, the rabbit's nails were removed and fixed in a paraformaldehyde solution for 24 h. The nails were then soaked in PLANK decalcification solution for 48 h. After 48 h, the nails were placed under tap water and rinsed continuously for 30 min to remove the residual solution of the PLANK decalcification solution from the nail surface.

Microscopic observation of rabbit nail tissue. The decalcified Con and Mod nail tissues were scraped, placed on sterile slides, fixed with drops of fixative, covered with coverslips, and placed under the microscope.

Histopathological sections of rabbit nails. The nails of decalcified Con, Mod, TBH–DMN, Gls–TBH-NE–DMN, and PC were made into paraffin-embedded sections, observed under the microscope, and photographed.[69,70]

Open Access Article. Published on 06 June 2025. Downloaded on 4/3/2026 4:50:10 AM. This article is licensed under a Creative Commons Attribution-NonCommercial 3.0 Unported Licence.

Statistical analysis

Statistical product and service solutions version 23.0 was used for all data analysis and processing. Data were subjected to a one-way analysis of variance. A p-value of less than 0.05 was considered indicative of statistical significance.

Results and discussion

Morphological characterization and insertion performance study of Gls–TBH-NE–DMN

The microstructure of Gls–TBH-NE–DMN prepared in this experiment featured a four-pronged conical design. The needle tip was intact and sharp, with no bending, breakage, or bubble generation. The tip of Gls–TBH-NE–DMN showed good compatibility with the backing layer; the tip of the needle was not separated from the backing layer, and the backing layer was flat without bubbles (Fig. 1b–e).

Table 1 Parafilm® insertion experiment results (n = 5)

Puncture layer	Holes	Puncture rate (%)	Average ± SD (%)
4	100	100	99.4 ± 1.5
4	99	99	
4	98	98	
4	100	100	
4	100	100	

Gls–TBH-NE–DMN was punctured into four layers of Parafilm®, with a puncture rate of 99.4% ± 1.5% when operated in parallel five times (Table 1). The relative error to the model prediction was <5%, suggesting that the prepared Gls–TBH-NE–DMN penetration rate was based on the experimental expectation, and the thickness of the skin stratum corneum and active epidermis layer was approximately 100 μm. The Gls–TBH-NE–DMN with a height of 800 μm in the present experiments had good mechanical strength and could successfully penetrate the skin stratum corneum and leave a drug delivery channel on the skin surface (Fig. 1f and g).

The Gls–TBH-NE–DMN tip bending increased with increasing weight (100–500 g), and the height of the Gls–TBH-NE–DMN was reduced from 800 to 698 ± 1.8 μm when the weight was 500 g, and the bending rate was approximately 12.75% ± 1.6%, suggesting that the prepared Gls–TBH-NE–DMN had good flexibility (Fig. 1h and i).

Results of dorsal mouse skin experiments of Gls–TBH-NE–DMN

The Gls–TBH-NE–DMN left a clear needle eye on the back of the mice, with a puncture rate of 95.7% ± 1.6%. This indicates that

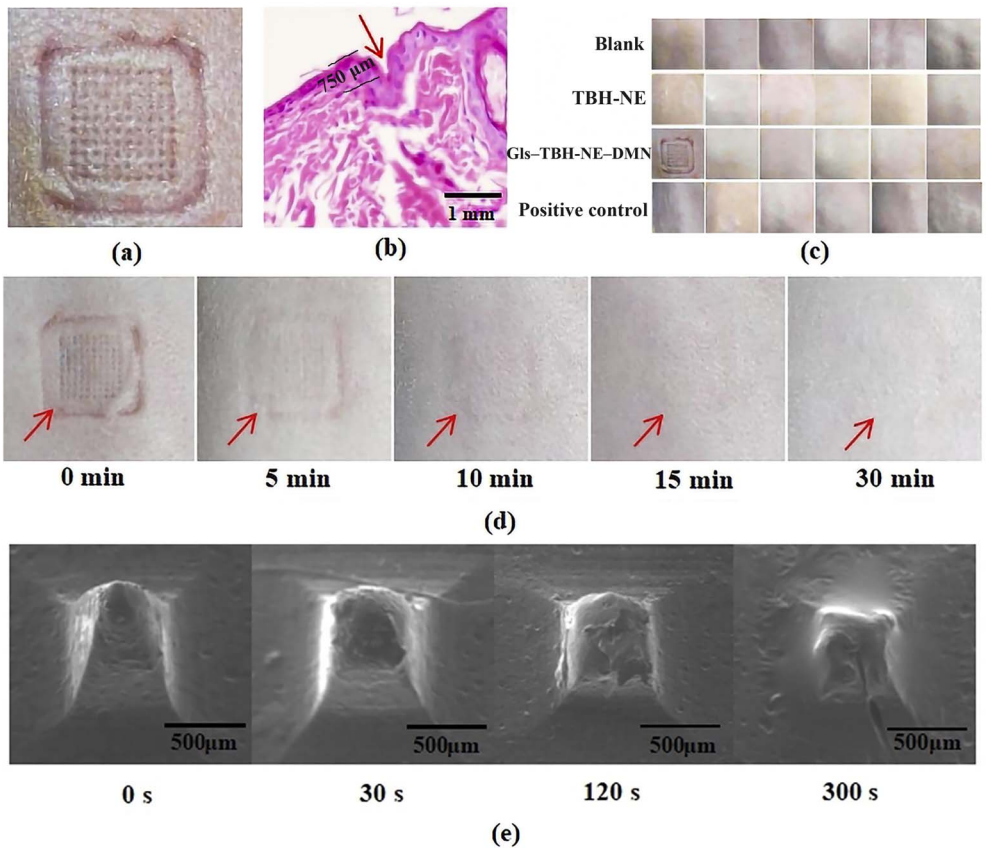

Fig. 2 Results of experiments on dorsal skin of mice with Gls–TBH-NE–DMN: (a) skin puncture experiments with Gls–TBH-NE–DMN, (b) histological sections of Gls–TBH-NE–DMN pricked mice skin, (c) skin irritation assessments of Gls–TBH-NE–DMN, (d) skin healing experiments with Gls–TBH-NE–DMN, and (e) intradermal dissolution experiments of Gls–TBH-NE–DMN.

 © 2025 The Author(s). Published by the Royal Society of Chemistry

Open Access Article. Published on 06 June 2025. Downloaded on 4/3/2026 4:50:10 AM. This article is licensed under a Creative Commons Attribution-NonCommercial 3.0 Unported Licence.

Gls–TBH-NE–DMN has good mechanical strength and can puncture the cuticle of the dorsal skin of mice. There was no erythema on the back skin of the mice, indicating that Gls–TBH-NE–DMN did not irritate the back skin of mice (Fig. 2a). The Gls–TBH-NE–DMN left luminal channels in the dorsal skin of mice, with a length of approximately 750 μm. The height of the Gls–TBH-NE–DMN prepared in this experiment was 800 μm, and the lengths of the needles in both instances were similar. This suggests that Gls–TBH–NE–DMN pierced the stratum corneum of the mouse back skin and left drug delivery channels on the skin surface (Fig. 2b).

The mice belonging to the TBH-NE, Gls–TBH-NE–DMN, and positive control groups did not exhibit irritation on their back skin. No erythema or edema was detected on the back skin of mice within 120 h, suggesting that TBH-NE and Gls–TBH–NE–DMN did not cause irritation to the back skin of mice and exhibited a good safety profile (Fig. 2c). After removing Gls–TBH-NE–DMN, the skin on the back of the mice showed clear pinholes, which disappeared after 30 min. No bleeding spots or redness were found in the dorsal skin of mice, suggesting that Gls–TBH-NE–DMN demonstrates sufficient safety (Fig. 2d).

The tip heights of Gls–TBH-NE–DMN at 0 s, 30 s, 120 s, and 300 s were observed from the top view using a FESEM, with the tip height at 0 s being 799.8 ± 0.2 μm, and the tip of Gls–TBH-NE–DMN almost disappearing at 300 s, with only the base of the backing layer remaining. This result indicated that the microneedle used in this experiment was a dissolving one (Fig. 2e).

DSC, FTIR, *in vitro* release, and *in vitro* transdermal permeation experiments of Gls–TBH-NE–DMN

The heat absorption peak of TBH appeared at 213.09 °C, the blank DMN had no heat absorption peak, and the physical mixture showed a TBH heat absorption peak at 210.30 °C, which indicated that the two were simply physically mixed. The heat absorption peak at 213.09 °C did not appear in Gls–TBH-NE–DMN, which indicated that TBH-NE was successfully loaded into DMN,[71] and Gls–TBH-NE–DMN was successfully prepared (Fig. 3a).

The FTIR spectra of the samples to be tested are shown in Fig. 3b. The FTIR spectrum of TBH showed characteristic absorption bands at 3035.41, 2962.13, 2217.74, 1631.48,

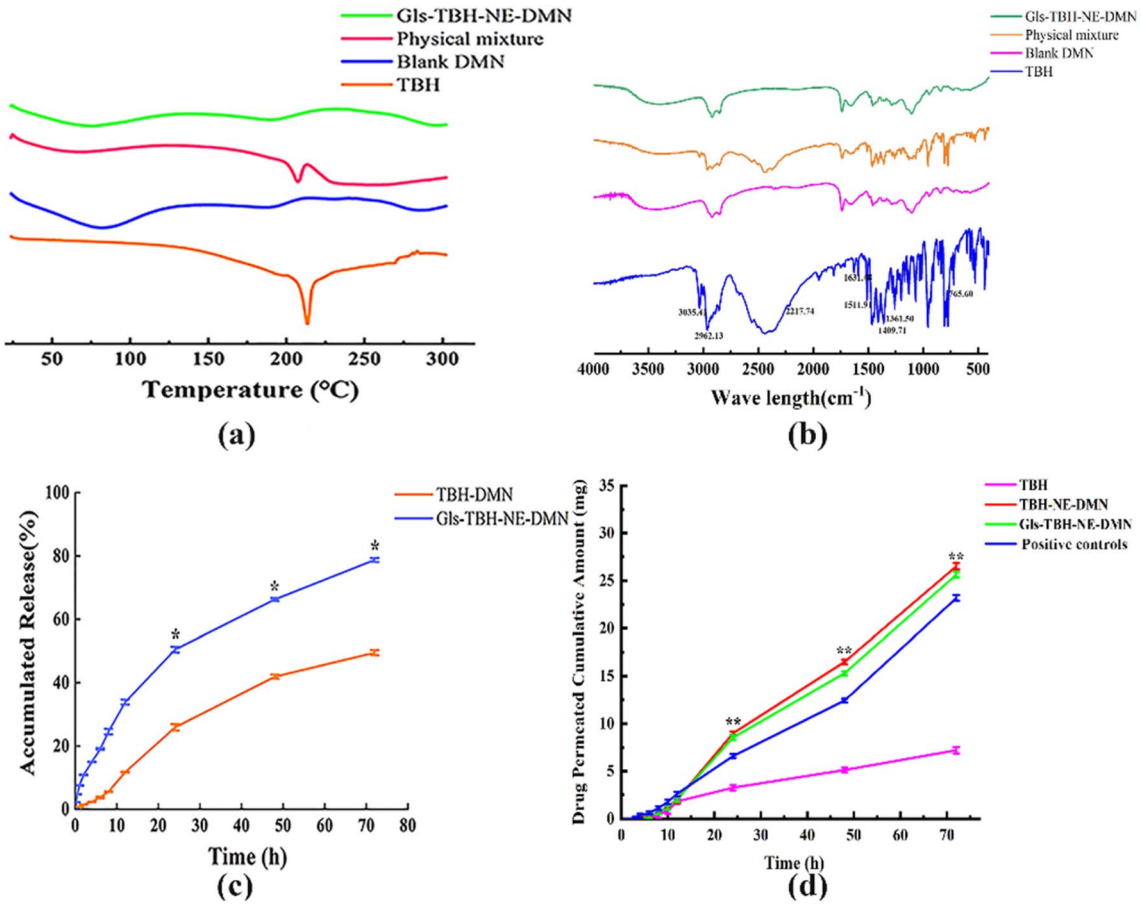

Fig. 3 Differential scanning calorimetry (DSC), Fourier transform infrared spectroscopy (FTIR), *in vitro* release degree and *in vitro* transdermal permeation experiments of Gls–TBH-NE–DMN: (a) DSC curves of Gls–TBH-NE–DMN, (b) FTIR spectra of Gls–TBH-NE–DMN, (c) *in vitro* release degree experiments of Gls–TBH-NE–DMN ($\bar{x} \pm s$, $n = 3$), (a statistically significant difference was observed between the TBH-DMN and Gls–TBH-NE–DMN groups (*$p < 0.05$), and (d) *in vitro* transdermal permeation experiments of Gls–TBH-NE–DMN ($\bar{x} \pm s$, $n = 3$), (significant differences were observed among groups (**$p < 0.01$), with TBH-NE-DMN, Gls–TBH-NE–DMN, and positive controls showing statistically significant variations compared with the TBH group).

Open Access Article. Published on 06 June 2025. Downloaded on 4/3/2026 4:50:10 AM. This article is licensed under a Creative Commons Attribution-NonCommercial 3.0 Unported Licence.

1511.91, 1409.71, 1361.50, and 765.60 cm^{-1}. At 3035.41 cm^{-1} for olefin C–H stretching and aromatic C–H stretching, 2962.13 cm^{-1} for alkane C–H stretching, 2217.74 cm^{-1} for alkyne C≡C stretching, and 1631.48 cm^{-1} for olefin C=C stretching, 1511.91 cm^{-1} for aromatic C=C bending, 1361.50 and 1409.71 cm^{-1} for alkane C–H bending, and 765.60 cm^{-1} for olefin C–H bending.

The FTIR spectra of the physical mixtures are the superposition of the TBH and blank DMN spectra, suggesting that the physical mixtures were simple mixtures of TBH and blank DMN. The FTIR spectra of Gls–TBH-NE–DMN and blank DMN were almost identical. When comparing the FTIR spectrum of Gls–TBH-NE–DMN with that of the physical mixture, the characteristic absorption peaks of TBH disappeared, but no new absorption peaks were generated, suggesting no chemical reaction between TBH and the carrier material in DMN. The two were simply hydrogen-bonded. The FTIR analysis results indicate that TBH-NE was successfully loaded into the DMN (Fig. 3b).

The analytical methodology of TBH release *in vitro* was established, with peak area (Y) as the ordinate and concentration (X) as the abscissa, and the linear regression equation was $Y = 185.8X + 369.8$ ($R^2 = 0.9993$), which showed that the concentration of TBH had a good linear relationship in the range of 10–120.00 μg mL^{-1}.

The *in vitro* cumulative release rate of TBH–DMN was 49.52% ± 0.80% after 72 h and that of Gls–TBH-NE–DMN was 78.74% ± 0.64% after 72 h. The seventy-two-hour *in vitro* cumulative release rate of Gls–TBH-NE–DMN was 1.59 times higher than that of TBH–DMN, suggesting that the binding of NE and DMN enhanced the *in vitro* release of TBH (Fig. 3c).

The data were fitted to zero-order, first-order, and Higuchi kinetic equations (Table 2). The experimental results showed that the *in vitro* cumulative release process of TBH–DMN within 72 h conformed to the zero-order kinetic equation, and the *in vitro* cumulative release of Gls–TBH-NE–DMN was based on the Higuchi equation.

The seventy-two-hour cumulative transdermal rates were 20.57% ± 0.98% for TBH, 75.77% ± 0.92% for TBH-NE–DMN, 73.21% ± 0.84% for Gls–TBH-NE–DMN, and 66.21% ± 0.86% for the positive control. The seventy-two-hour cumulative transdermal rates of TBH-NE–DMN and Gls–TBH-NE–DMN were 3.56 times higher than that of TBH, suggesting that NE binds to DMN and increases the cumulative transdermal permeability of TBH. The disadvantages of poor water solubility and skin penetration of TBH were overcome (Fig. 3d).

Table 2 Fitting equations for cumulative release time models of TBH–DMN and Gls–TBH-NE–DMN *in vitro*[a]

Group	Model	Model fitting equation	r
TBH–DMN	Zero-order kinetic	$Q_n^* = -0.1479 + 07986t$	$r = 0.9847$
	First-order kinetic	$Q_n^* = 63\,326.1420 \times (1 - e^{-1.1495t})$	$r = 0.9630$
	Higuchi	$Q_n^* = 2.4089t^{1/2} - 1.2646$	$r = 0.8174$
Gls–TBH-NE–DMN	Zero-order kinetic	$Q_n^* = -0.1265 + 1.6247t$	$r = 0.8024$
	First-order kinetic	$Q_n^* = 71.7346 \times (1 - e^{-0.0638t})$	$r = 0.9626$
	Higuchi	$Q_n^* = 9.4226t^{1/2} - 2.6617$	$r = 0.9965$

[a] Terbinafine hydrochloride dissolving microneedles (TBH–DMN), dissolving microneedles of terbinafine hydrochloride nanoemulsion for beta-1,3-glucanase (Gls–TBH-NE–DMN).

Table 3 Fitting equations for the *in vitro* TBH, TBH-NE–DMN, Gls–TBH-NE–DMN, and positive control cumulative percutaneous transdermal transition time models[a]

Group	Model	Model fitting equation	r
TBH	Zero-order kinetic	$Q_n^* = -1.2994 + 0.3286t$	$r = 0.9844$
	First-order kinetic	$Q_n^* = -1.6832 \times (1 - e^{0.0376t})$	$r = 0.8453$
	Higuchi	$Q_n^* = 3.0305t^{1/2} - 6.0601$	$r = 0.9908$
TBH-NE–DMN	Zero order kinetic	$Q_n^* = -3.2042 + 1.0746t$	$r = 0.9924$
	First-order kinetic	$Q_n^* = -4.8614 \times (1 - e^{0.0404t})$	$r = 0.8809$
	Higuchi	$Q_n^* = 8.8406t^{1/2} - 15.3263$	$r = 0.9538$
Gls–TBH-NE–DMN	Zero-order kinetic	$Q_n^* = -3.5685 + 1.0216t$	$r = 0.9916$
	First-order kinetic	$Q_n^* = -10.2447 \times (1 - e^{0.0301t})$	$r = 0.9442$
	Higuchi	$Q_n^* = 8.6097t^{1/2} - 16.2757$	$r = 0.9424$
Positive controls	Zero-order kinetic	$Q_n^* = -2.6199 + 0.8722t$	$r = 0.9934$
	First-order kinetic	$Q_n^* = -32.99 \times (1 - e^{0.0153t})$	$r = 0.9922$
	Higuchi	$Q_n^* = 7.5612t^{1/2}$–14.0204	$r = 0.9577$

[a] Terbinafine hydrochloride (TBH), dissolving microneedles of terbinafine hydrochloride nanoemulsion (TBH-NE–DMN), dissolving microneedles of terbinafine hydrochloride nanoemulsion for beta-1,3-glucanase (Gls–TBH-NE–DMN).

© 2025 The Author(s). Published by the Royal Society of Chemistry

Open Access Article. Published on 06 June 2025. Downloaded on 4/3/2026 4:50:10 AM. This article is licensed under a Creative Commons Attribution-NonCommercial 3.0 Unported Licence.

The data were fitted to zero-order, first-order, and Higuchi kinetic equations (Table 3). The experimental results showed that the process of *in vitro* cumulative percutaneous transmittance of TBH within 72 h conformed to the Higuchi equation, the process of *in vitro* cumulative percutaneous transmittance of TBH-NE–DMN, Gls–TBH-NE–DMN, and the positive control conformed to the zero-order kinetic equation.

In vitro fungal inhibition experiment of Gls–TBH-NE–DMN

Antifungal sensitivity study of Gls–TBH-NE–DMN. In this experiment, the MIC values of TBH–DMN, Gls–TBH-NE–DMN, and PC solutions against *C. albicans* were determined. The fungal strains in the Mod group grew all over the medium; the TBH–DMN group still had more fungal strains growing at 512

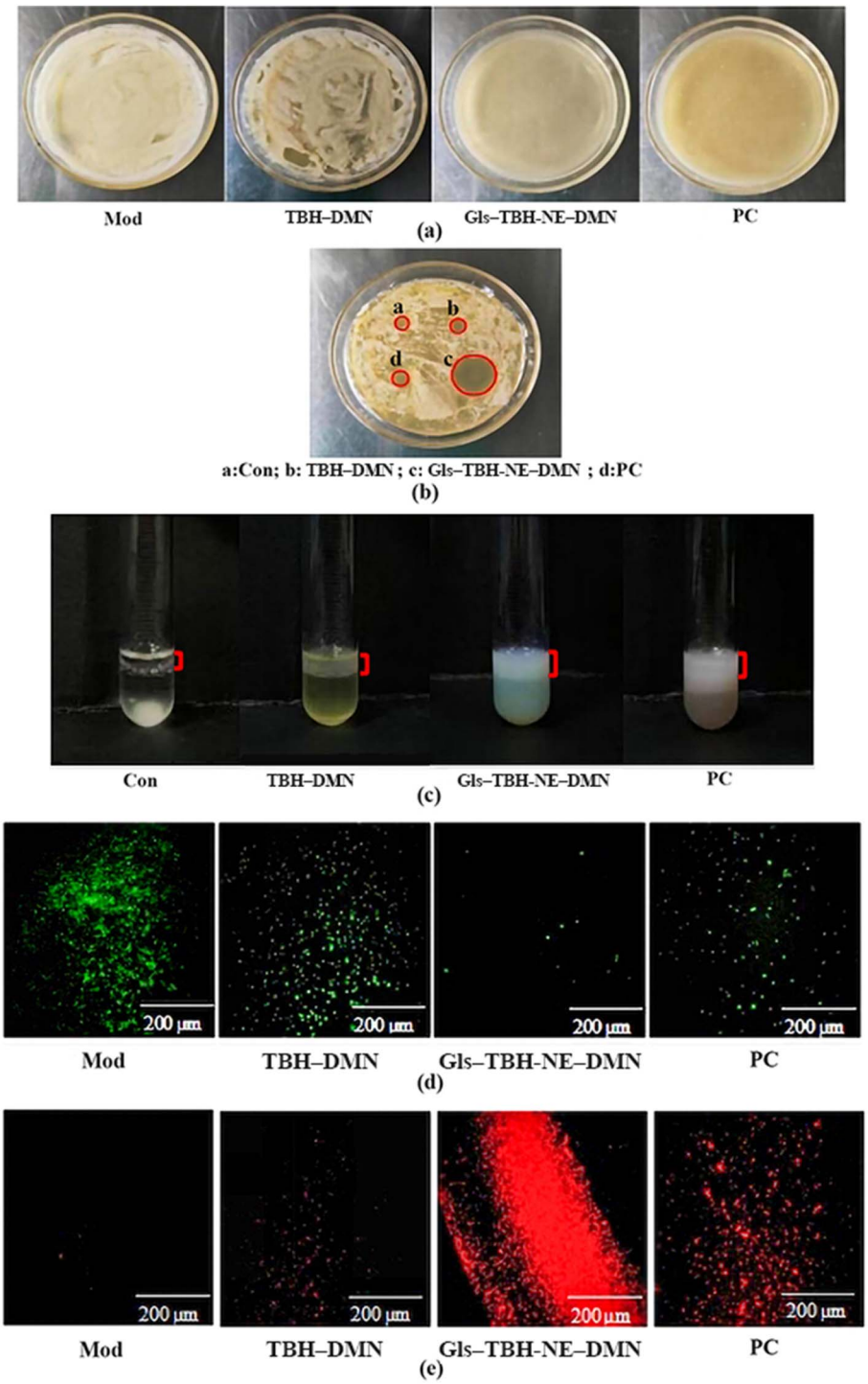

Fig. 4 *In vitro* fungal inhibition experiments of Gls–TBH-NE–DMN: (a) and (b) antifungal susceptibility studies of Gls–TBH-NE–DMN, (c) fungal cell wall synthesis inhibition experiments of Gls–TBH-NE–DMN, and (d and e) fungal biofilm permeation and inhibition experiments of Gls–TBH-NE–DMN.

© 2025 The Author(s). Published by the Royal Society of Chemistry

Open Access Article. Published on 06 June 2025. Downloaded on 4/3/2026 4:50:10 AM. This article is licensed under a Creative Commons Attribution-NonCommercial 3.0 Unported Licence.

Table 4 Drug sensitivity paper test results[a]

Drug	Inhibition circle diameter (mm)
(a) Con groups	6
(b) TBH–DMN groups	7
(c) Gls–TBH-NE–DMN groups	17.5
(d) PC groups	8

[a] Terbinafine hydrochloride dissolving microneedles (TBH–DMN), dissolving microneedles of terbinafine hydrochloride nanoemulsion for beta-1,3-glucanase (Gls–TBH-NE–DMN).

$\mu g\ mL^{-1}$, and the inhibition effect was poor. Gls–TBH-NE–DMN significantly inhibited fungal growth at a concentration of 512 $\mu g\ mL^{-1}$, and PC had fewer colonies growing at a concentration of 512 $\mu g\ mL^{-1}$. In conclusion, Gls–TBH-NE–DMN administered at a concentration of 512 $\mu g\ mL^{-1}$ showed a significant antifungal effect with the growth of less than three colonies, suggesting an MIC of 512 $\mu g\ mL^{-1}$ (Fig. 4a).

The inhibitory effects of TBH–DMN, Gls–TBH-NE–DMN, and PC solution against *C. albicans* are shown in Table 4. The circle of inhibition was the largest in the Gls–TBH-NE–DMN, which was larger than that in the PC and TBH–DMN, and the inhibitory effect on *C. albicans* was significant (Fig. 4b).

Fungal cell wall synthesis inhibition experiments of Gls–TBH-NE–DMN. There was no emulsification in the Con; slight but insignificant emulsification was observed in TBH–DMN. There was significant emulsification in Gls–TBH-NE–DMN, whereas in PC since the original solution was the flocculent solution, the white flocculent solution can be observed in the figure partially overlapping with the emulsification phenomenon and producing slight delamination. In conclusion, the emulsification results of Gls–TBH-NE–DMN were similar to those of PC, and the height of the foam produced was similar. Gls–TBH-NE–DMN inhibited the production of fungal cell walls and exerted an inhibitory effect (Fig. 4c).

Fungal biofilm permeation and inhibition experiments of Gls–TBH-NE–DMN. Mod showed a large amount of green fluorescence, suggesting that a large number of fungal biofilms were formed in this experimental group. TBH–DMN showed more green fluorescence, suggesting that a certain amount of fungal biofilms were formed in this experimental group. Gls–TBH-NE–DMN showed extremely little green fluorescence, suggesting that few fungal biofilms were formed in this experimental group. PC showed less green fluorescence, suggesting some fungal biofilm formation in this experimental group. Therefore, from the results of FITC-ConA staining, Gls–TBH-NE–DMN had the highest number of apoptotic fungal cells, suggesting that Gls–TBH-NE–DMN had the optimal effect in inhibiting fungal biofilm formation (Fig. 4d).

Mod had almost no red fluorescence, suggesting no fungal apoptosis in this experimental group. TBH–DMN had less red fluorescence, suggesting a small amount of fungal apoptosis in this experimental group. Gls–TBH-NE–DMN showed a large amount of red fluorescence, suggesting a large number of fungal cell apoptosis in this experimental group. PC showed

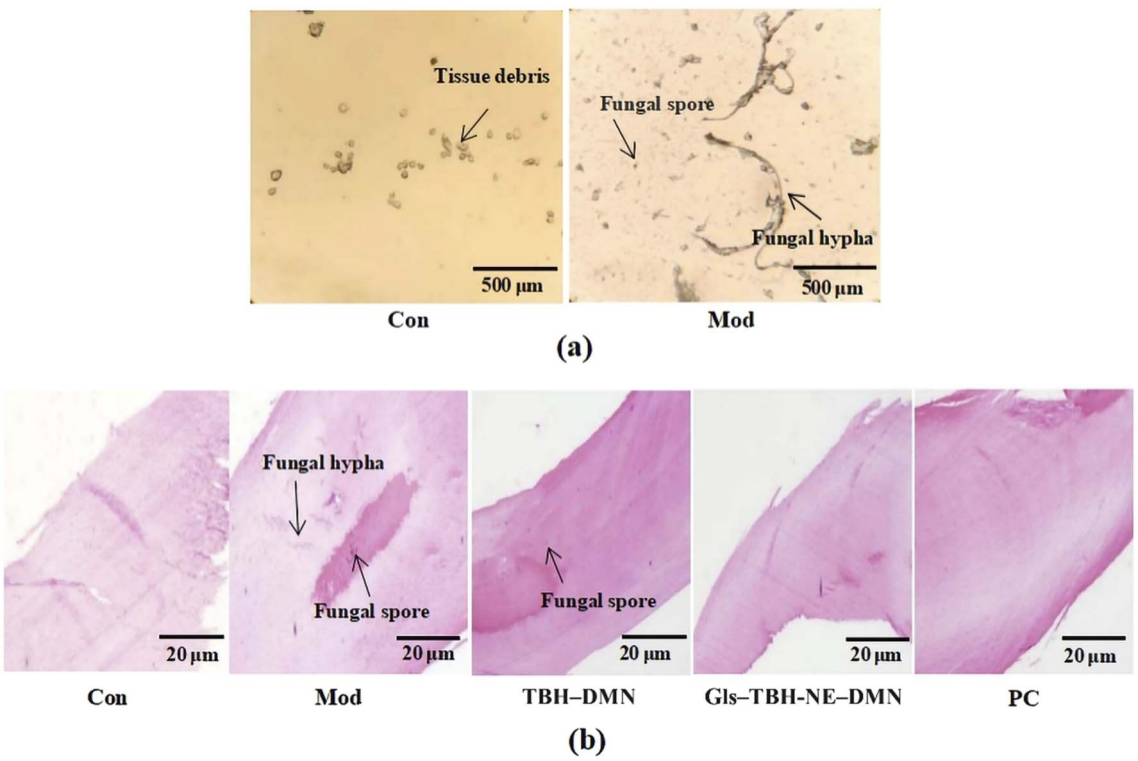

Fig. 5 *In vivo* fungal inhibition experiments of Gls–TBH-NE–DMN: (a) microscopic observations of rabbit nail tissues and (b) histopathological results of rabbit nail sections.

© 2025 The Author(s). Published by the Royal Society of Chemistry

Open Access Article. Published on 06 June 2025. Downloaded on 4/3/2026 4:50:10 AM. This article is licensed under a Creative Commons Attribution-NonCommercial 3.0 Unported Licence.

some red fluorescence, suggesting some fungal apoptosis. Therefore, as shown by the results of PI fluorescence staining, the Gls–TBH-NE–DMN group exhibited the most significant red fluorescence and the highest number of fungal cell apoptosis. The Gls–TBH-NE–DMN disrupted the fungal biofilms, and the antifungal drug TBH smoothly entered the cell to exert its inhibitory effect (Fig. 4e).

In the *in vivo* bacterial inhibition experiments, Gls–TBH-NE–DMN and the positive controls exerted similar therapeutic effects. This indicates that the prepared microneedles can inhibit bacterial growth. Microneedles have great advantages for clinical treatment. Microneedles can penetrate the stratum corneum, and their transdermal ability is stronger than that of ordinary creams. Additionally, microneedles are conveniently used to avoid drug contamination.

***In vivo* fungal inhibition experiments of Gls–TBH-NE–DMN.** No fungal mycelium or spore growth was found in the nail tissue of Con. In the nail tissue of Mod, fungal hyphae and spores were abundant, demonstrating the success of fungal infection in the rabbit nail model (Fig. 5a).

The Con had healthy tissue growth under the nail plate without infection, and the Mod had clear fungal spore clusters and fungal hyphae growth under the nail plate. There were few fungal spores in TBH–DMN, suggesting that it inhibited fungal spore growth to some extent. There was almost no fungal spore or hyphae growth in Gls–TBH-NE–DMN and PC. From the experimental results, the treatment effect of Gls–TBH-NE–DMN was similar to that of PC, and there were no fungal spores or mycelium growth in the nail tissues, suggesting that Gls–TBH-NE–DMN inhibited the growth of fungi and exerted a fungistatic effect (Fig. 5b).

Conclusion

In this study, for the first time, the preferred therapeutic agents for fungal infections, TBH and β-1,3-glucan inhibitor Gls, along with a dual-carrier dissolution microneedle patch, were microfabricated to prepare microneedle patches. The skin puncture experiments and mice skin tissue sections showed that Gls–TBH-NE–DMN punctured the skin stratum corneum and left drug delivery channels on the skin surface. The results of the skin healing test and skin irritation evaluation showed that Gls–TBH-NE–DMN was nonirritating to the skin and had a good safety profile. The DSC and FTIR studies demonstrated that TBH-NE was successfully loaded into the DMN. The *in vitro* release degree experiment showed that the accumulative release degree of Gls–TBH-NE–DMN at 72 h *in vitro* was 1.59 times that of TBH–DMN, suggesting that the binding of NE to DMN enhanced the *in vitro* release of TBH. *In vitro* transdermal permeation experiments showed that the 72 h cumulative transdermal permeability of Gls–TBH-NE–DMN was 3.56 times that of TBH, suggesting that the binding of NE to DMN enhanced the cumulative transdermal rate of TBH.

The results of the *in vitro* antifungal susceptibility test showed that the lowest inhibitory concentration of Gls–TBH-NE–DMN against *C. albicans* was 512 μg mL^{-1}. The results of the fungal cell wall synthesis inhibition experiments showed that Gls–TBH-NE–DMN can effectively inhibit fungal cell wall synthesis and destroy the barrier effect of the fungal cell wall to drugs. The results of fungal biofilm permeation and inhibition experiments showed that Gls–TBH-NE–DMN destroyed the formation of C.albicans cell wall and biofilm and damaged the protective effect of the fungal cell wall and biofilm on fungal cells, thus allowing TBH to enter fungal cells to exert its inhibitory effect. *In vivo* fungal inhibition experiments showed that the selection of *C. albicans* to establish an onychomycosis model was successful. Histopathological sections of rabbit nails showed that Gls–TBH-NE–DMN patches were administered through the proximal nail folds of rabbit nails, exerting an *in vivo* fungal inhibitory effect, which was consistent with the results of *in vitro* fungal inhibition experiments.

Discussion

As the outermost protective layer of fungal cells, the cell wall can reduce fungal cell sensitivity to antifungal drugs, thereby contributing to suboptimal antifungal treatment efficacy. By utilizing the mechanism of β-1,3-glucanase (Gls) to inhibit the synthesis of β-1,3-glucan, the assembly of the fungal cell wall can be significantly disrupted,[72] thereby enhancing the susceptibility of fungal cells to drug treatment.[73–78] In this study, Gls and TBHs were delivered using DMN as a drug carrier. Based on the characteristics of the proximal subungual type of infection, Gls–TBH-NE–DMN was applied to the proximal nail fold site of the nail to deliver antifungal drugs directly to the subcutaneous nail matrix area for antifungal treatment at the source of fungal infections to improve the drawbacks of oral and topical treatments for onychomycosis. The experimental results of this study show that Gls–TBH-NE–DMN punctured the stratum corneum of the skin and left drug delivery channels on the skin surface. The prepared Gls–TBH-NE–DMN effectively inhibited the growth of fungal cells and exerted fungal inhibition by inhibiting the formation of fungal cell walls and destroying the fungal biofilm protection of fungal cells.

In recent years, microneedles have been used as delivery carriers for transdermal drug preparations, with the characteristics of enabling drugs to pass smoothly through the stratum corneum and enter directly into the skin, forming a drug delivery channel, accelerating drug absorption, and exerting therapeutic effects.[79] Owing to the in-depth research on microneedles in related fields, the use of their special structure effectively improves the penetration of different types of drugs, especially in the treatment of chronic diseases, immune system diseases, skin tumors, and other diseases. Microneedles can deliver biomacromolecules, biosmall molecules, and water-soluble drugs. Upon insertion into the skin, the DMN needle tip can spontaneously degrade and release the loaded drug, which is directly absorbed by the skin, thereby achieving precise drug delivery. In transdermal drug delivery, DMN can not only serve as a carrier to load drugs and their intermediates but also significantly increase the transdermal permeability of drugs. In addition, the tiny channels formed on the skin surface by DMN can heal themselves in a short time, effectively reducing the risk of infection caused by the breakage of traditional solid needle

Open Access Article. Published on 06 June 2025. Downloaded on 4/3/2026 4:50:10 AM. This article is licensed under a Creative Commons Attribution-NonCommercial 3.0 Unported Licence.

tips, making the drug more effective in disease treatment and achieving painless, minimally invasive and efficient treatment.[80–82]

The new transdermal TBH drug delivery formulation developed in this study remains in the laboratory research stage. The micro-mold casting technique adopted by the research group can merely meet the requirements of the laboratory preparation phase. Furthermore, during the *in vivo* antibacterial experiment, although the rabbits were anesthetized, there exists potential for improvement in the methodology used for claw removal within the context of antibacterial research. While this study can still be refined and improved, it introduces a pioneering approach in which TBH-NE was co-loaded with Gls in DMN to create a dual-loaded transdermal microneedle patch aimed at treating nail fungal infections. The successful preparation of this dosage form provides new ideas for the treatment of nail fungal diseases and new research directions for the development of new dosage forms of antibacterial drugs.

Ethics approval

This study was conducted in accordance with the principles outlined in the Declaration of Helsinki. Ethical approval was obtained from the Ethics Committee of Jiamusi University (No. JMSU-2024041701). All institutional and national guidelines for the care and use of laboratory animals were strictly adhered to.

Data availability

The datasets generated and analyzed during this study are not publicly available but are available from the corresponding author upon reasonable request.

Author contributions

Yan Wang and Wang Huilin prepared and characterized microneedles. Jianing Liu conducted *in vitro* release experiments and high-performance liquid analysis. Yan Wang and Wang Huilin conducted strain and animal-related experiments. Yang Ping, Yu Zhang and Weitong Sun designed the whole experiment. Yonghua Qi and Hongbin Qiu provided technical guidance regarding the experiment. Yang Ping, Yan Wang and Wang Huilin discussed and prepared the manuscript with the contributions of all authors.

Conflicts of interest

The authors have no relevant financial or non-financial interests to disclose.

Acknowledgements

This work was supported by the Basic Research Support Program for Excellent Young Teachers in Heilongjiang Province (YQJH2023216), North Medicine and Functional Food Characteristic Subject Project in Heilongjiang Province (No. HLJTSXK-2022-03), and Basic Research Fund for Excellent Innovation Teams in Higher Education Institutions in Heilongjiang Province (2023-KYWF-0640).

References

1 N. M. Martinez-Rossi, N. T. A. Peres, T. A. Bitencourt, M. P. Martins and A. Rossi, *J. Fungi*, 2021, **7**(8), 629.
2 S. R. Lipner and R. K. Scher, *J. Am. Acad. Dermatol.*, 2019, **80**(4), 853–867.
3 C. R. Stewart, L. Algu, R. Kamran, C. F. Leveille, K. Abid, C. Rae and S. R. Lipner, *J. Am. Acad. Dermatol.*, 2021, **85**(5), 1227–1239.
4 I. Haghani, M. Shams-Ghahfarokhi, A. Dalimi Asl, T. Shokohi and M. T. Hedayati, *Mycoses*, 2019, **62**(2), 128–143.
5 S. Sen, S. N. Borah, A. Bora and S. Deka, *Biotechnol. Rep.*, 2020, **27**, e00516–e00524.
6 S. Gregoriou, M. Kyriazopoulou, A. Tsiogka and D. Rigopoulos, *J. Fungi*, 2022, **8**(10), 1079–1093.
7 H. M. Zhu and H. Wen, *Chin. J. Mycol.*, 2020, **15**(06), 374–377.
8 M. E. R. Lopes, T. A. Bitencourt, P. R. Sanches, M. P. Martins, V. M. Oliveira, A. Rossi and N. M. Martinez-Rossi, *J. Fungi*, 2022, **8**(8), 878–889.
9 J. Thomas, G. M. Peterson, J. K. Christenson, S. Kosari and K. E. Baby, *Am. J. Ther.*, 2019, **26**(3), e388–e396.
10 A. K. Gupta, M. Venkataraman and M. Talukder, *Drugs Aging*, 2022, **39**(3), 191–198.
11 A. P. Krawczyk-Santos, R. N. Marreto, A. Concheiro, C. Alvarez-Lorenzo and S. F. Taveira, *Int. J. Pharm. X*, 2022, **4**, 100118–100131.
12 A. K. C. Leung, J. M. Lam, K. F. Leong, K. L. Hon, B. Barankin, A. A. M. Leung and A. H. C. Wong, *Recent Pat. Inflammation Allergy Drug Discovery*, 2020, **14**(1), 32–45.
13 A. K. Gupta, N. Stec, R. C. Summerbell, N. H. Shear, V. Piguet, A. Tosti and B. M. Piraccini, *J. Eur. Acad. Dermatol. Venereol.*, 2020, **34**(9), 1972–1990.
14 J. M. Falotico, S. R. Lipner and C. C. Investig, *Dermatology*, 2022, **15**, 1933–1957.
15 J. Hu, S. Y. Zhang, W. G. Zhang, Z. H. Yan and H. M. Li, *Chin. J. Mycol.*, 2022, **17**(01), 22–26.
16 L. Zhang, F. Z. Li, Z. F. Ou, Q. Li, M. P. Huang and J. Y. Yu, *Dermatol. Venereol.*, 2022, **44**(02), 155–156.
17 S. Nerome, N. Yokota, Y. Ojima and M. Azuma, *J. Microbiol. Methods*, 2021, **190**, 106327–106347.
18 Y. Tan, M. Leonhard, S. Ma, D. Moser and B. Schneider-Stickler, *Microb. Pathog.*, 2017, **113**, 342–347.
19 K. Martin, B. M. McDougall, S. McIlroy, J. Chen and R. J. Seviour, *FEMS Microbiol. Rev.*, 2007, **31**(2), 168–192.
20 A. K. Gupta and K. A. G. Foley, *Ital. Dermatol. Venereol.*, 2019, **154**(1), 50–55.
21 S. Carradori, A. Ammazzalorso, B. De Filippis, A. F. Şahin, A. Akdemir, A. Orekhova, G. Bonincontro and G. Simonetti, *Antibiotics*, 2022, **11**(10), 1375–1393.
22 N. Toukabri, S. Corpologno, M. E. Bougnoux, D. El Euch, N. Sadfi-Zouaoui and G. Simonetti, *Mycoses*, 2018, **61**(2), 79–87.

© 2025 The Author(s). Published by the Royal Society of Chemistry

Open Access Article. Published on 06 June 2025. Downloaded on 4/3/2026 4:50:10 AM. This article is licensed under a Creative Commons Attribution-NonCommercial 3.0 Unported Licence.

23 F. Y. Gu, J. Gao, H. Ruan and G. Q. He, *Chin. J. Food Sci.*, 2012, **12**(008), 135–140.
24 M. Suriani Ribeiro, R. Graciano de Paula, A. Raquel Voltan, R. G. de Castro, C. B. Carraro, L. José de Assis, A. Stecca Steindorff, G. H. Goldman, R. N. Silva, C. J. Ulhoa and V. Neves Monteiro, *Biomolecules*, 2019, **9**(12), 781–797.
25 T. N. Ferreira, J. B. Barufi, P. A. Horta, D. P. Castro and F. A. Genta, *An. Acad. Bras. Cienc.*, 2021, **93**(3), e20191402–e20191408.
26 M. Steger, M. Bermejo-Jambrina, T. Yordanov, J. Wagener, A. A. Brakhage, V. Pittl, L. A. Huber, H. Haas, C. Lass-Flörl, W. Posch and D. Wilflingseder, *Virulence*, 2019, **10**(1), 957–969.
27 Y. Tan, S. Ma, T. Ding, R. Ludwig, J. Lee and J. Xu, *Front. Microbiol.*, 2022, **13**, 815091–815099.
28 Y. Tan, S. Ma, M. Leonhard, D. Moser and B. Schneider-Stickler, *Int. J. Biol. Macromol.*, 2018, **108**, 942–946.
29 J. Y. Wu, Q. P. Ming and H. T. Pan, *China Med. Guide*, 2020, **18**(03), 181.
30 S. Yazdanpanah, F. Sasanipoor, H. Khodadadi, A. Rezaei-Matehkolaei, F. Jowkar, K. Zomorodian, M. Kharazi, T. Mohammadi, S. Nouripour-Sisakht, R. Nasr and M. Motamedi, *Int. J. Derm.*, 2023, **62**(1), 120–127.
31 B. Chen, Y. Sun, J. Zhang, R. Chen, X. Zhong, X. Wu, L. Zheng and J. Zhao, *Front. Microbiol.*, 2019, **10**, 1228–1236.
32 A. Tavakkol, J. C. DuBois and A. K. Gupta, *Antimicrob. Agents Chemother.*, 2024, **68**(10), e0068224.
33 N. I. Elsherif, R. N. Shamma and G. Abdelbary, *AAPS PharmSciTech*, 2017, **18**(2), 551–562.
34 S. T. Tanrıverdi, S. Hilmioğlu Polat, D. Yeşim Metin, G. Kandiloğlu and Ö. Özer, *J. Liposome Res.*, 2016, **26**(2), 163–173.
35 C. A. Roque-Borda, L. M. D. G. Primo, K. P. Medina-Alarcón, I. C. Campos, C. F. Nascimento, M. M. S. Saraiva, A. Berchieri Junior, A. M. Fusco-Almeida, M. J. S. Mendes-Giannini, J. Perdigão, F. R. Pavan and F. Albericio, *Adv. Sci.*, 2025, **12**(1), e2410893.
36 K. Sylla, R. C. K. Tine, D. Sow, S. Lelo, M. Dia, S. Traoré, B. Faye and T. Dieng, *J. Fungi*, 2019, **5**(2), 35.
37 F. F. Veiga, L. V. de Castro-Hoshino, P. S. T. Rezende, M. L. Baesso and T. I. E. Svidzinski, *Exp. Dermatol.*, 2022, **31**(11), 1810–1814.
38 R. G. Gouveia, N. R. Oliveira, F. P. Andrade-Júnior, R. C. Ferreira, G. M. W. Amorim, D. K. F. Silva, S. S. Duarte, C. I. S. Medeiros, A. A. Oliveira-Filho and E. O. Lima, *Braz. J. Biol.*, 2023, **83**, e271530.
39 T. da Rosa Pinheiro, G. A. Dantas, J. L. G. da Silva, D. B. R. Leal, R. B. da Silva, T. A. de Lima Burgo, R. C. V. Santos and B. A. Iglesias, *Pharmaceutics*, 2023, **15**(5), 1511.
40 I. L. E. Barros, F. F. Veiga, L. V. de Castro-Hoshino, M. Souza, A. M. Malacrida, B. V. Diniz, R. S. Dos Santos, M. L. Bruschi, M. L. Baesso, M. Negri and T. I. E. Svidzinski, *Antibiotics*, 2022, **12**(1), 72.
41 S. Yazdanpanah, A. Jabrodini, M. Motamedi, K. Zomorodian, M. Kharazi, S. Shabanzadeh, F. Ghasemi, S. Shariat and M. Rezaei Arab, *Antonie Van Leeuwenhoek*, 2023, **117**(1), 6.
42 R. X. Shen, Z. Z. Zhu, J. Y. Zhang and H. F. Luo, *World Clin. Drugs*, 2017, **38**(09), 638–642.
43 W. Y. Cui and J. Wang, *Micro-Nano Electron. Technol.*, 2023, **60**(2), 195–204.
44 X. Yang, W. Cao, X. Gu, L. Zheng, Q. Wang, Y. Li, F. Wei, T. Ma, L. Zhang and Q. Wang, *Int. J. Pharm.*, 2023, **647**, 123543.
45 C. Zhang, L. K. Vora, I. A. Tekko, F. Volpe-Zanutto, K. Peng, A. J. Paredes, H. O. McCarthy and R. F. Donnelly, *Int. J. Pharm.*, 2023, **642**, 123108.
46 K. Braz Gomes, B. D'Souza, S. Vijayanand, I. Menon and M. J. D'Souza, *Int. J. Pharm.*, 2022, **613**, 121393.
47 T. Waghule, G. Singhvi, S. K. Dubey, M. M. Pandey, G. Gupta, M. Singh and K. Dua, *Biomed. Pharmacother.*, 2019, **109**, 1249–1258.
48 R. Zhang, J. Yang, Q. Luo, J. Shi, H. Xu and J. Zhang, *Drug Delivery*, 2022, **29**(1), 2217–2233.
49 M. Kumari and D. K. Nanda, *Burns*, 2023, **49**(5), 1003–1016.
50 U. Gul, M. I. Khan, A. Madni, M. F. Sohail, M. Rehman, A. Rasul and L. Peltonen, *Drug Delivery*, 2022, **29**(1), 600–612.
51 Z. Baharvandi, A. Salimi, R. Arjmand, A. Jelowdar and A. Rafiei, *AAPS PharmSciTech*, 2022, **23**(7), 280.
52 V. Dupuis, C. Cerbu, L. Witkowski, A. V. Potarniche, M. C. Timar, M. Żychska and C. M. Sabliov, *Drug Delivery*, 2022, **29**(1), 1007–1024.
53 X. Hou, H. Wang, X. Yao, Q. Zhou and X. Niu, *ACS Nano*, 2025, **19**(18), 17709–17727.
54 Y. Xie, Z. Wu, J. Wang, Z. Li and Z. Hu, *ACS Appl. Mater. Interfaces*, 2025, **17**(17), 25152–25162.
55 S. Sun, X. Liu, X. Meng, Z. Yang, X. Zhang and H. Dong, *ACS Nano*, 2025, **19**(15), 15109–15119.
56 J. Hu, D. Zhang, S. Chen, X. Wang, Z. Zheng, S. Gui and N. He, *Eur. J. Pharm. Biopharm.*, 2025, **211**, 114717.
57 L. K. Vora, A. J. Courtenay, I. A. Tekko, E. Larrañeta and R. F. Donnelly, *Int. J. Biol. Macromol.*, 2020, **146**, 290–298.
58 M. J. Garland, E. Caffarel-Salvador, K. Migalska, A. D. Woolfson and R. F. Donnelly, *J. Control. Release*, 2012, **159**(1), 52–59.
59 C. Diedrich, I. C. Zittlau, N. M. Khalil, A. F. G. Leontowich, R. A. Freitas, I. Badea and R. M. Mainardes, *Pharmaceutics*, 2023, **15**(6), 1592.
60 C. B. Tripathi, P. Parashar, M. Arya, M. Singh, J. Kanoujia, G. Kaithwas and S. A. Saraf, *Drug Delivery Transl. Res.*, 2018, **8**(5), 1313–1334.
61 Q. Sun, Y. Li, J. L. Li, S. H. Yang and D. X. Zheng, *Beijing Stomatol.*, 2011, **19**(2), 4.
62 A. Ghose, B. Nabi, S. Rehman, S. Md, N. A. Alhakamy, O. A. A. Ahmad, S. Baboota and J. Ali, *Polymers*, 2020, **12**(12), 2903.
63 X. C. Li, *Study on the antifungal activity of salvinorin against Candida albicans and Cryptococcus neoformans and its mechanism of action*, Shanxi University of Science and Technology, 2022.
64 L. F. Zhang, *Study on the effect of light-activated disinfection on mixed biofilms of Candida albicans and Candida tropicalis*, Hebei Medical University, 2022.

Open Access Article. Published on 06 June 2025. Downloaded on 4/3/2026 4:50:10 AM.
This article is licensed under a Creative Commons Attribution-NonCommercial 3.0 Unported Licence.

65 X. Liu, *Study on the potentiating effect of CGA-derived antimicrobial peptide bCAT against Candida albicans biofilm*, Chongqing Medical University, 2021.
66 Q. Jiang, *V-type proton pump regulates the cariogenicity of Candida albicans-streptococcus mutans biofilm and its mechanism*, Chongqing Medical University, 2022.
67 F. Endringer Pinto, C. Bagger, G. Kunze, N. Joly-Tonetti, J. P. Thénot, H. Osman-Ponchet and C. Janfelt, *Mycoses*, 2020, **63**(8), 869–875.
68 T. Shimamura, N. Kubota, S. Nagasaka, T. Suzuki, H. Mukai and K. Shibuya, *Antimicrob. Agents Chemother.*, 2011, **55**(7), 3150–3155.
69 A. K. Gupta, E. A. Cooper, T. Wang, S. A. Lincoln and W. L. Bakotic, *J. Fungi*, 2023, **9**(6), 671.
70 K. L. Chen and M. A. Hinshaw, *J. Cutaneous Pathol.*, 2023, **50**(2), 103–105.
71 A. Romeo, A. Bonaccorso, C. Carbone, G. Lupo, C. Daniela Anfuso, G. Giurdanella, C. Caggia, C. Randazzo, N. Russo, G. L. Romano, C. Bucolo, M. Rizzo, G. Tosi, J. Thomas Duskey, B. Ruozi, R. Pignatello and T. Musumeci, *Int. J. Pharm.*, 2022, **627**, 122195.
72 S. Nerome, N. Yokota, Y. Ojima and M. Azuma, *J. Microbiol. Methods*, 2021, **190**, 106327.
73 T. Q. Wei and M. S. Liu, *Chin. J. Mycol.*, 2022, **17**(4), 324–329.
74 M. Suriani Ribeiro, R. Graciano de Paula, A. Raquel Voltan, R. G. de Castro, C. B. Carraro, L. José de Assis, A. Stecca Steindorff, G. H. Goldman, R. N. Silva, C. J. Ulhoa and V. Neves Monteiro, *Biomolecules*, 2019, **9**(12), 781.
75 T. N. Ferreira, J. B. Barufi, P. A. Horta, D. P. Castro and F. A. Genta, *An. Acad. Bras. Cienc.*, 2021, **93**(3), e20191402.
76 M. Steger, M. Bermejo-Jambrina, T. Yordanov, J. Wagener, A. A. Brakhage, V. Pittl, L. A. Huber, H. Haas, C. Lass-Flörl, W. Posch and D. Wilflingseder, *Virulence*, 2019, **10**(1), 957–969.
77 Y. Tan, S. Ma, T. Ding, R. Ludwig, J. Lee and J. Xu, *Front. Microbiol.*, 2022, **24**(13), 815091.
78 Y. Tan, S. Ma, M. Leonhard, D. Moser and B. Schneider-Stickler, *Int. J. Biol. Macromol.*, 2018, **108**, 942–946.
79 S. Mdanda, P. Ubanako, P. P. D. Kondiah, P. Kumar and Y. E. Choonara, *Polymrs*, 2021, **13**(15), 2405–2428.
80 L. Song, J. Chi, Z. Li, Y. Tao, Y. Sun, Q. Zhou, S. Lu, Q. Huang, S. Huang, X. Lu, M. Wu, Y. Yang, L. Chen, X. Li, K. Shi and J. Xiao, *Int. J. Pharm.*, 2023, **643**, 123215.
81 X. Wang, Y. Ma, X. Qi, X. Ruan, D. Cao and F. Zhao, *Int. J. Pharm.*, 2023, **644**, 123340.
82 M. Xing, X. Wang, L. Zhao, Z. Zhou, H. Liu, B. Wang, A. Cheng, S. Zhang and Y. Gao, *Int. J. Pharm.*, 2021, **600**, 120406.

© 2025 The Author(s). Published by the Royal Society of Chemistry